Geochemistry, Petrology and Mineralogy of Coal Measure Shales in the Middle Jurassic Yanan Formation from Northeastern Ordos Basin, China: Implications for Shale Gas Accumulation

CHEN Qian[1, *], YAN Xiangbin[1], GUO Yuanling[1], HONG Taiyuan[1], NIE Haikuan[1], ZHANG Jinchuan[2, 3], TANG Xuan[2, 3], LI Wanjun[4] and LIU Chong[5]

1 *SINOPEC Petroleum Exploration and Production Institute, Beijing 100083, China*
2 *Key Laboratory of Shale Gas Exploration and Evaluation, Ministry of Land and Resources, China University of Geosciences, Beijing 100083, China*
3 *School of Energy and Resources, China University of Geosciences, Beijing 100083, China*
4 *CNPC Economic & Technology Research Institute, Beijing 100724, China*
5 *Henan Institute of Geological Survey, Zhengzhou 450001, China*

Abstract: The Jurassic Yanan Formation is one of the most important coal-producing formations and hydrocarbon source rocks in the Ordos Basin, North China. To evaluate the shale gas potential of the Yanan shale, a total of 48 samples from north Ordos Basin were sampled, and their geochemical, petrological, mineralogical and pore characteristics were investigated. It was found that the shale samples are a suite of early mature source rock. The total organic carbon (TOC) content ranges from 0.33% to 24.12% and the hydrogen index (HI) ranges from 43.31mg/g to 330.58 mg/g. The relationship between T_{max} and HI indicates the organic matter is type Ⅱ-Ⅲ. This conclusion is also supported by the organic petrological examination results, which shows that the kerogen is mainly liptinite and vitrinite. Minerals in the samples are composed mainly of quartz, clay and feldspar, and the clay minerals are composed of prevailing kaolinite, illite/smectite, chlorite and a small amount of illite. Under scanning electron microscope, OM pores in the Yanan shale are scarce except pores come from the kerogen intrinsic texture or clay aggregates within the organic particles. As the weak compaction caused by shallow burial depth, interparticle pores and intraparticle pores are common, the hydrocarbon storage capacity of the Yanan shale was improved. According to evaluation, the Yanan shale is considered as a good shale gas reservoir, but its hydrocarbon potential is more dependent on biogenic and coal-derived gas as the thermogenic gas is limited by the lower thermal maturity.

Keywords: geochemistry, mineralogy, shale gas, Yanan Formation, Ordos Basin

1 Introduction

Unconventional oil and gas resources have become much important in the global energy industry with the development of petroleum exploration and production technologies. Coal and organic matter-rich shale, which have been identified as source rocks in petroleum geology, are also considered as feasible reservoirs in recent years. Hydrocarbon resources in these self-storage reservoirs are usually defined as continuous-type accumulation (Schmoker, 2002) and differ in both storage mechanism and production strategy from conventional oil and gas exploration. With the renewal concept on hydrocarbon reservoir and successful practice aiming at hydrocarbon in organic rich shale, oil/gas exploitation target has been greatly extended (Nie Haikuan and Jin Zhijun, 2016), and consequently, it is necessary to reevaluate the hydrocarbon potential of formations containing high-quality source rocks.

The Ordos Basin is a multi-cycle superimposed basin and an important natural gas source area in North China. It not only has the largest gas field (He Zixin et al., 2003) of China at present, but also is one of the primary coal-bed methane target areas (Tang Shuheng et al., 2004; Shao

* Corresponding author. E-mail: chenqian.syky@sinopec.com

Longyi et al., 2015). During the transformation of depositional environments from Paleozoic to Mesozoic, three suites of coal-bearing formations, including the paralic Permo-Carboniferous, continental Triassic formations and Jurassic formations, were deposited. According to the geological researches, these coal-bearing formations were identified as the main source rocks in the Ordos Basin (Miao Jianyu et al., 2005; Hanson et al., 2007). The Permian coal and organic-rich shale is not only the main source of tight gas fields (Bian Congsheng et al., 2015), but also an important coal-bed methane reservoir (Feng Sanli, 2002; Tang Shuheng et al., 2004; Shao Longyi et al., 2015; Zhang Yongsheng et al., 2017). In addition, it is the most promising paralic coal-bearing shale gas reservoir in North China (Zhang Jinchuan et al., 2007, 2016; Zou Caineng et al., 2010; Wang Shejiao et al., 2011; Jiang et al., 2016; Dang et al., 2016; Hao Ziguo et al., 2017). The Yanchang lacustrine black shale is a good oil source rock for many commercial oil fields (Ji et al., 2014) and has been proven to contain huge hydrocarbon resources (Tang et al., 2014; Wang Xiangzeng et al., 2014; Yang et al., 2015; Liu et al., 2016). Shale in the Jurassic coal-bearing formation, though it is also considered as a good source rock (Li Zixue et al., 2014; Hanson et al, 2007), has been rarely studied so far. A few studies have previously characterized its organic property (Han Zongyuan et al., 2007; Hanson et al., 2007; Huang Wenhui et al., 2010; 2011), however, little attention has been paid to the possibility of being a shale gas reservoir.

In this study, the organic geochemical and petrological characteristics, mineral composition, microstructure and pores of the Yanan shale samples from north Ordos Basin were analyzed. The main purposes of this paper are to (1) evaluate the source rock quality and (2) discuss the potential of the Yanan shale as a shale gas reservoir. Under the circumstances that most of the current shale gas researches are focusing on marine formations, the study on the Yanan coal-bearing shale will be a supplement to the understanding on shale gas.

2 Geological Settings

The Ordos Basin, with an area of 26×10^4 km^2, locates at the central part of the North China Plate. Under the whole geological history of the North China Plate, the evolution of the Ordos Basin can be divided into five stages: aulacogen in the middle-late Proterozoic, shallow sea tableland in the early Paleozoic, coastal plains in the late Paleozoic, inland lake in the Mesozoic and fault depression in the Cenozoic (Yang et al., 2005; Wang Shejiao et al., 2011). The depositional environments have undergone a sequentially marine-terrestrial transition from Paleozoic to Mesozoic (Yang et al., 2005), and correspondingly, the lithology of the Paleozoic-Mesozoic strata in the Ordos Basin can be generally characterized as the Cambrian-Ordovician shallow marine carbonate, Permo-Carboniferous transitional shale and Triassic-Jurassic terrestrial coal-bearing shale (Zhang et al., 1997; Hanson et al., 2007; Wang Shejiao et al., 2011; Tang Xuan et al., 2012).

During the Late Triassic, the Indosinian tectonic movement enabled the Ordos Basin to become a stable subsidence basin and also further accelerated the transitional sedimentary environments converting to terrestrial facies (Zhang et al., 1997). After the deposition of Yanchang Formation, the original depocenter at the southwest Ordos Basin uplifted. As a result, the new depocenter of the Yanan Formation transferred to a relative lower part of the basin's center, which is the current Yanan region. The depositional facies of the Yanan period varies northwestward from lacustrine, delta to fluvial (Fig. 1). Our study area is located at the Northeast Ordos Basin and across two structural zones: the North Yimeng uplift and the Central Yishan Slope (Xiao et al., 2005; Jiang et al., 2012; Tang et al., 2014). The Yanan Formation at the study area is mainly deposited in an alluvial plain environment (Fig. 1) and is considered as a favor zone of the Yanan low metamorphic coal-bed methane (Zhang Peihe, 2007).

Based on the data of several boreholes, the Yanan Formation, with a total thickness of 150–250 m, is composed mainly of shale, sandstone and coal (Fig. 2). Aside from one layer at the top, black shales mostly occur as thin layers intercalated with coal. Grey shales prevail and usually contain a certain percentage of silty or sandy materials. Plant stems, leafs or charcoal fragments can be commonly observed in grey shales as well as some sandstones.

3 Samples and Methods

Thirty-eight core samples and ten outcrops from the Yanan Formation were selected and examined in this study, including eleven black carbonaceous shales with visible plant fragments, sixteen dark grey-black homogeneous shales and twenty-one grey-dark grey silty or sandy shales. The samples were obtained from three boreholes located at the Taijizhao Township, Ejin Horo Qi, Ordos city and the outcrops are from the Jungar Qi, Ordos City (Fig. 1). In this study, several fundamental properties for shale gas accumulation, such as organic geochemistry and petrology, mineralogy and pore structure (Jarvie et al., 2007), were preliminarily investigated by laboratory tests.

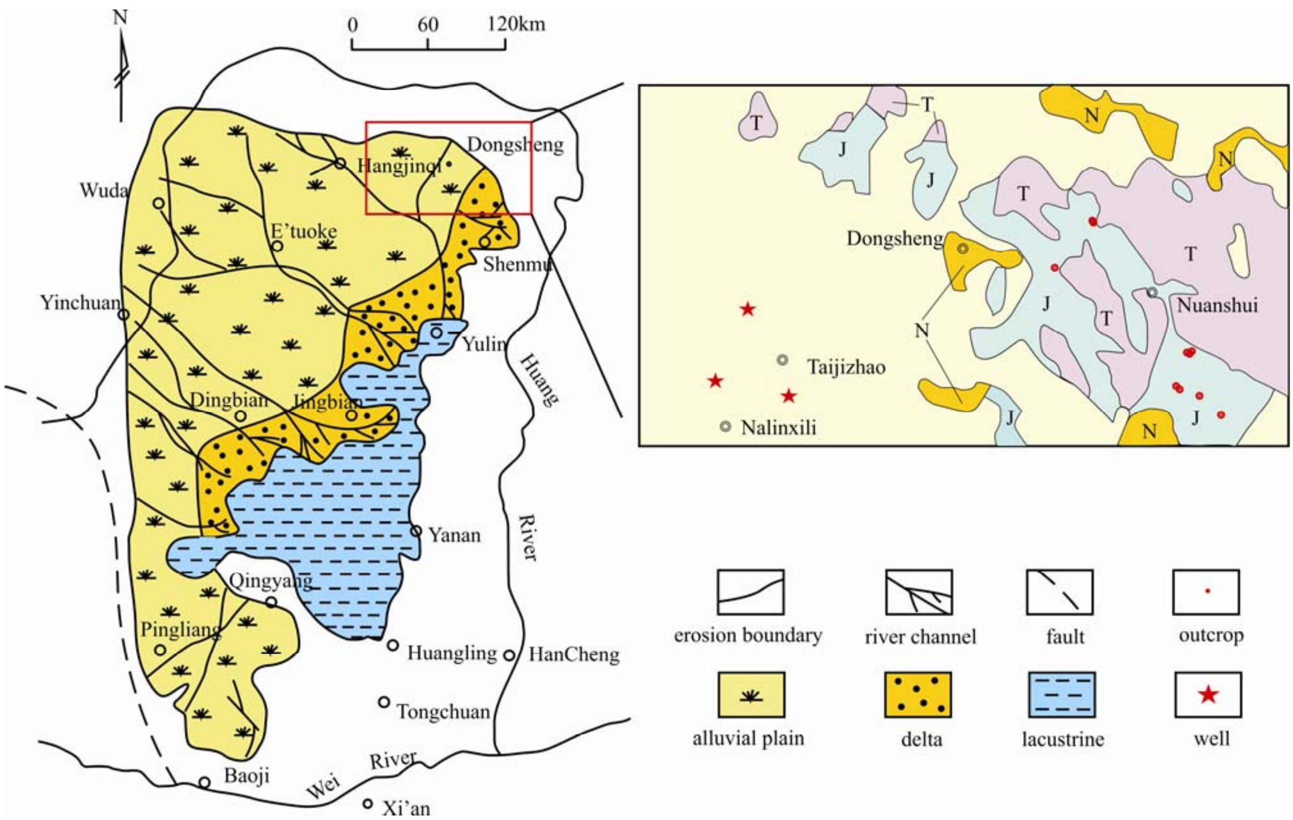

Fig. 1. Sedimentary environment of the Yanan Formation in the Ordos Basin (sedimentary environment map was modified from Wang Shejiao, 2011), and outcrop exposure map show distribution of core wells and outcrops in the study area.

The total organic carbon (TOC) content and Rock-Eval pyrolysis parameters were measured separately by a Leco C230 carbon analyzer and a Rock-Eval 6 instrument. Through Rock-Eval pyrolysis, the free hydrocarbon (S_1 mg HC/g rock), hydrocarbon-generating potential (S_2 mg HC/g rock), and peak temperature during S_2 generation (T_{max}) were measured. Corresponding hydrogen index (HI) and production index (PI) were calculated in accordance with Behar et al. (2001).

The organic petrological characteristics were examined by observing isolated kerogen under transmitted light and fluorescence using an optical microscope. The type of the organic matter was identified following the Chinese Oil and Gas Industry Standard of SY/T 5152-2014, in which macerals are classified into four basic groups: sapropelinite, liptinite, vitrinite and inertinite. The relative percent of the macerals were measured based on 300 particles counts for each sample and the organic matter type was determined using both the ternary plate (Hou Dujie and Zhang Linye, 2003) and the equation of organic type index (TI) as described as Cao Qingying (1985). A MPV-SP microphotometer was used to determine the vitrinite reflectance (R_o) which is a general thermal maturity indicator. More than 25 maximum reflectance values were measured for each sample and the vitrinite reflectance in this paper was reported as the mean value.

X-ray diffraction (XRD) was used to analyze the mineral composition of the shale samples using a Bruker D8-Discover X-ray diffractometer. Quantitative estimation of the mineral content was conducted following the Standard of SY/T 5163-2010. Ar-ion milling and Field emission scanning electron microscope (FE-SEM) techniques were combined to observe the microstructure and the pore structure. The milling was conducted parallel to the bedding using a Gatan Ilion II 697 milling system. Both before and after slightly Au coating (Leica EM SCD5000 High Resolution Sputter Coater), the milled surface was observed using a Hitachi S8010 scanning electron microscope under accelerating voltage of 10 kV and an energy disperse spectroscopy (EDS) was used to identify minerals. All the images were taken under secondary electron (SE) mode with back-scatter signal. The procedure has been discussed in detail in Chen et al. (2016). To quantitatively evaluate the pore system, low-pressure N_2 adsorption (LNA) was also applied to determine the surface area, pore volume and pore size distribution. A Quadrasorb SI apparatus was performed under low-pressure condition (<127 kPa) at 77 K. The surface area and pore volume were calculated using the multi-point BET equation (Braunauer et al., 1940) and Brunauer, Emmett, and Teller (BJH) (Barrett et al., 1951) model, respectively.

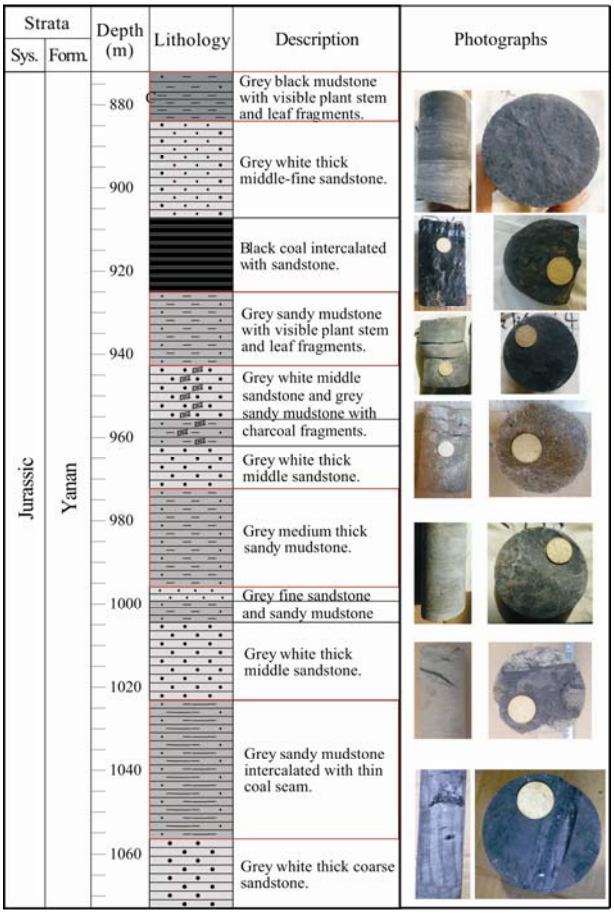

Fig. 2. Lithology and sample photographs of the Yanan Formation in well X6-2 (the sampling sections are outlined by the red box).

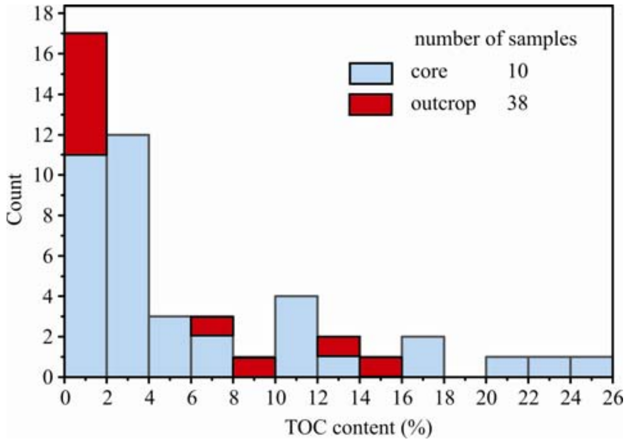

Fig. 3. Frequency distribution histogram of TOC content.

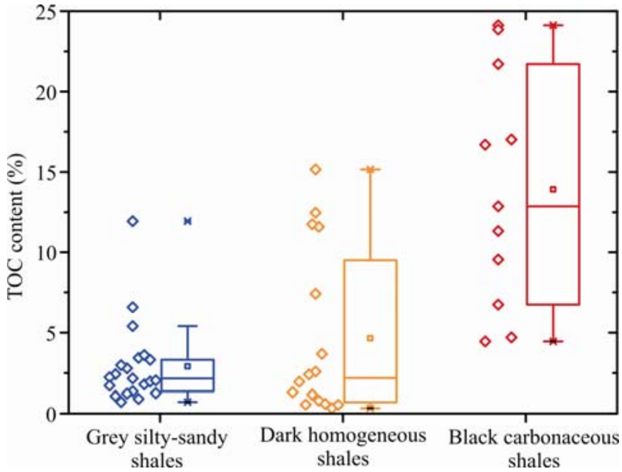

Fig. 4. Box-chart of TOC content of shale samples in lithology.

4 Results

4.1 Organic geochemistry

Total organic carbon (TOC) content of the 48 shale samples ranges from 0.33% to 24.12% (Table 1). Wherein, the TOC content of the ten outcrops ranges from 0.33% to 15.16% with an average of 4.79%, whereas that of the core samples ranges from 0.72% to 24.12% with an average of 6.33%. The statistical column is bimodal with two peaks locating at 2% and 10%–12% (Fig. 3). For more than half of the samples (29), the TOC content is lower than 4%, while a quarter of them (12) have TOC content higher than 10%.

Different rocks classified based on hand-specimen observation are found to be related to organic matter richness (Fig. 4). The TOC contents of grey silty or sandy shale samples are generally concentrated into the interval from 1% to 3% and only three of these samples have TOC content higher than 5%. Dark homogeneous shales are similar with silty-sandy shales but have a wider range of TOC content and a little higher proportion of organic-rich samples. TOC contents of the black carbonaceous shale samples are the highest and majority of them are higher than 5%.

Free hydrocarbon (S_1) yielded in the shale samples from the pyrolysis ranges from 0.01 mg/g to 1.21 mg/g and the potential hydrocarbon (S_2) ranges from 0.37 mg/g to 33.77 mg/g (Table 1). Statistically, the core samples exhibit both higher S_1 and S_2 content than the outcrop samples (Table 1), and that suggests the residual hydrocarbon and hydrogen in the OM of the outcrops were decreased by weathering (Tan et al., 2014). The peak pyrolysis temperature (T_{max}) varies in a small interval between 426°C and 439°C, indicating that the samples are mostly matured source rocks just entering the oil-generating window. Hydrogen index (HI) ranges from 43.31 mg/g to 330.58 mg/g. The cross plot of T_{max} versus HI suggests that the organic matter in the samples is mainly Ⅱ-Ⅲ type (Fig. 5).

4.2 Organic petrology

Under the transmitted light, the identification of organic matter is basically dependent on their occurrence, morphology and transparency. According to the

Table 1 Total organic carbon (wt%) and rock-eval pyrolysis parameters of shale samples

Sample ID	Sample Type	Lithology	TOC (%)	Rock-Eval pyrolysis parameters				
				S_1 (mg HC/g rock)	S_2 (mg HC/g rock)	T_{max} (°C)	HI (mg HC/g OM)	PI
NP02DH04-1	Outcrop	DHS	12.47					
NP07DH11-2	Outcrop	DHS	0.81					
DHND2001	Outcrop	DHS	1.17	0.02	1.12	433	95.73	0.02
DHND2012	Outcrop	DHS	0.60	0.02	0.37	434	61.67	0.05
DHND1006	Outcrop	DHS	0.54	0.02	0.47	434	87.04	0.04
NP06DH08-1	Outcrop	DHS	0.56	0.02	0.67	437	119.64	0.03
NP01DH12-1	Outcrop	BCS	9.55					
NP01DH14-4	Outcrop	BCS	6.75	0.19	7.14	428	105.78	0.03
BP01DH5-2	Outcrop	DHS	15.16					
BP01DH15-2	Outcrop	DHS	0.33					
X1-2-20	Core	GSS	1.38	0.02	1.42	436	102.90	0.01
X1-2-19	Core	BCS	17.01					
X1-2-18	Core	DHS	7.42					
X1-2-21	Core	BCS	24.12					
X1-2-17	Core	DHS	11.59	0.05	5.02	434	43.31	0.01
X1-2-16	Core	GSS	5.41	0.11	10.48	426	193.72	0.01
X1-2-14	Core	GSS	2.17					
X1-2-15	Core	GSS	2.80	0.08	2.74	429	97.86	0.03
X1-2-12	Core	GSS	3.44					
X1-2-13	Core	GSS	2.99	0.06	4.14	435	138.46	0.01
X1-2-11	Core	DHS	2.59					
X1-2-10	Core	GSS	3.62	0.06	3.40	435	93.92	0.02
X1-2-9	Core	GSS	2.43					
X1-2-8	Core	GSS	1.23					
X1-2-7	Core	BCS	12.86	1.21	33.63	435	261.51	0.03
X1-2-22	Core	DHS	3.68					
X1-2-25	Core	GSS	0.91					
X1-2-26	Core	DHS	1.32					
X1-2-27	Core	GSS	6.59					
X1-2-28	Core	GSS	3.32					
X1-2-29	Core	GSS	0.72	0.09	0.52	442	72.22	0.15
X1-2-30	Core	DHS	11.74					
X1-2-31	Core	BCS	23.86					
X1-2-32	Core	GSS	2.24	0.07	2.44	434	108.93	0.03
X1-2-33	Core	GSS	1.80	0.05	2.30	435	127.78	0.02
X1-2-34	Core	GSS	1.08	0.03	1.98	434	183.33	0.01
X1-2-35	Core	GSS	1.97	0.04	2.68	435	136.00	0.01
JX1-1	Core	BCS	16.69	0.16	17.97	431	107.67	0.01
JX1-3	Core	GSS	1.72	0.34	2.26	439	131.40	0.13
JX1-4	Core	DHS	1.96	0.09	3.55	435	181.12	0.02
JX1-5	Core	GSS	2.05	0.08	4.45	429	217.07	0.02
JX1-6	Core	DHS	2.42	0.14	8.00	429	330.58	0.02
JX1-7	Core	BCS	4.71	0.13	12.72	430	270.06	0.01
JX2-7	Core	BCS	4.46	0.1	4.53	433	101.57	0.02
X5-3-28	Core	BCS	21.71	0.53	33.77	430	155.55	0.02
X5-3-22	Core	GSS	1.26	0.01	1.92	435	152.38	0.01
X6-2-21	Core	GSS	11.93					
X5-3-16	Core	BCS	11.32					

Notes: HC, Hydrocarbon; OM, Organic matter; PI, Production index; DHS, Dark homogeneous shale; BCS, Black carbonaceous shale; GSS, Grey silty-sandy shale.

occurrence, the organic particles in the Yanan shale samples are classified as amorphous organic matter (AOM) and morphological organic matter (MOR).

Most of the AMO from the Yanan kerogen are brown in color under transmitted light and show weak or no fluorescence (Figs. 6a and b). These organic particles are identified as humic AOM which is originated from alteration of higher plants or benthic algae by bacteria. In the samples, cutinite is another type of OM showing fluorescence (Figs. 6c and d). Though not common, the cuticle in the liptinite group is also observed, and can be identified through its unique ductile and folded appearance and moderate fluorescence (Fig. 6e).

The MOR organic matter particles have clear outlines and sometimes they retain part of the original structure of plants (Figs. 6f and g). Some of them are brown-reddish brown in color and have irregular shapes with sharp corners (Figs. 6f, g and h), and others are totally opaque black and exhibit more simple morphology (Figs. 6i and j). These two kinds of MOR are separately recognized as vitrinite and inertinite groups (Guan et al., 2016).

According to quantitative statistics of kerogen macerals, the liptinite and vitrinite groups are most abundant and contribute more than 80% of the organic matter in the samples (Table 2). The liptinite content varies from 38% to 72% with an average of 56%, and the vitrinite content varies from 13% to 41% with an average of 30%. The content of Sapropelinite plus inertinite is generally less

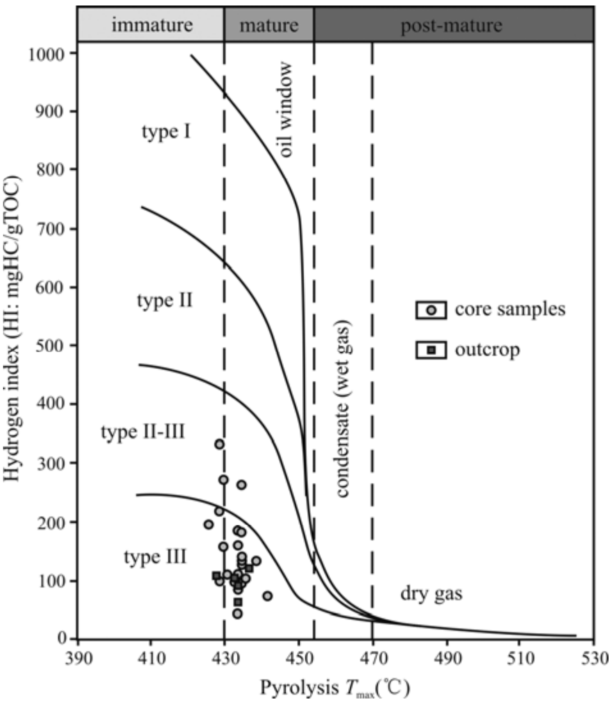

Fig. 5. Organic matter type and hydrocarbon generation stage defined by plots of pyrolysis T_{max} to hydrogen index (HI) (modified from Makeen et al. (2015)).

than 10%. The type index (TI) of the organic matter ranges from −22.5 to 31.25 (Table 2), indicating that about half of the samples have type Ⅲ kerogen while the other half have type II_2 kerogen which is comparable to the Ⅱ-Ⅲ organic matter determined by using pyrolysis parameters (Fig. 5). This outcome also agrees well with the organic matter type determined by the ternary plate (Fig. 7).

The vitrinite reflectance of the shale samples ranges in a small interval from 0.48% to 0.60% (Table 2). This interval also fits with the T_{max} according to the conversion equation between this two maturity parameters (Wüst, 2013). Nevertheless, no obvious positive relationship was found between R_o and T_{max} in the study area. Interestingly, R_o exhibit a negative relationship with TI (Fig. 8). Previous studies suggest this relationship is probably a sign of suppression of R_o caused by amorphous-rich kerogen (Price and Baker, 1985). The more hydrogen-rich macerals, such as sapropel components (Hulton and Cook, 1980; Xie and Qiu, 2005; Tang et al., 2016), liptinite (Kalkreuth, 1982; Raymond and Murchison, 1991) or even hydrogen-rich vitrinite (Hao and Chen, 2010; Zhang Juan, 2017) exist in the kerogen, the lower the R_o becomes. Therefore, the unexpected high liptinite content mostly resulted from humic AOM in the Yanan samples is probably the cause of this relationship, and the R_o values may be underestimated or inaccurate. Lo et al., (1993) has established a R_o-HI plate to correct R_o with high hydrogen in maceral, and the plate suggests there is small discrepancy between the measured R_o and correction values. As the Yanan shale has relatively low HI (generally lower than 300 mg/g) and the R_o generally fit with the level of T_{max}, the underestimation of R_o is probably slight.

4.3 Mineralogy

Mineral composition is one of the most important factors with respect to hydrocarbon storage and production in shales (Bowker, 2007). Previous studies have proved that mineral composition can affect the pore space (Schieber, 2010; Loucks et al., 2012; Gupta et al., 2013; Zuo Zhaoxi, 2017), hydrocarbon adsorption capacity (Ji et al., 2012; Heller and Zoback, 2014) and mechanical property (Sone and Zoback, 2013; Kumar et al., 2015; Nicolás-López and Valdiviezo-Mijangos, 2016) of shale.

According to the XRD results (Table 3 and Fig. 9), the Yanan shale samples mainly consist of quartz, feldspar, clay and a minor amount of carbonate mineral. The quartz content ranges from 30.92% to 59.40% with an average of 40.18%. The K-feldspar content ranges from 1.93% to 13.78% with an average of 5.14% and the plagioclase content ranges from 1.59% to 20.63% with an average of 9.59%. The clay mineral is composed of kaolinite, chlorite, illite/smectite mixed layer and illite, and the total clay content ranges from 31.27% to 47.31% with an average of 41.47%. The kaolinite and illite/smectite are generally prevailing in the Yanan shale samples and the content of both chlorite and illite are generally no more than 10%.

The provenance of the Yanan Formation, according to Huang Gang et al. (2009), is granitoids, gneiss system and epi-metamorphic rocks from the Yin Mountain at the northern boundary of the Ordos Basin, which can explain why the feldspar content in the shale samples is high. An overall negative relationship is found between quartz and feldspar (Fig. 10). Due to the fact that feldspar is much more volatile than quartz during weathering, their relationship has been usually used as an indicator of sedimentary rocks' weathering intensity (Pettijohn, 1975) that varies with transported distance (time) and climate (Kuhn and Diekmann, 2002; Andersson et al., 2004). With increasing distance from the source area, the fraction of quartz in the sum of feldspar and quartz increase because of less atmospheric contributions of volcanic ash (Jones and Blatt, 1984). Therefore, the negative relationship may be explained as a result of the fluctuation of transportation and climate. Another possible reason which can be directly linked to this negative relationship is that the dissolution of feldspar generally releases additional silica for authigenic quartz forming during diagenesis (Jones and

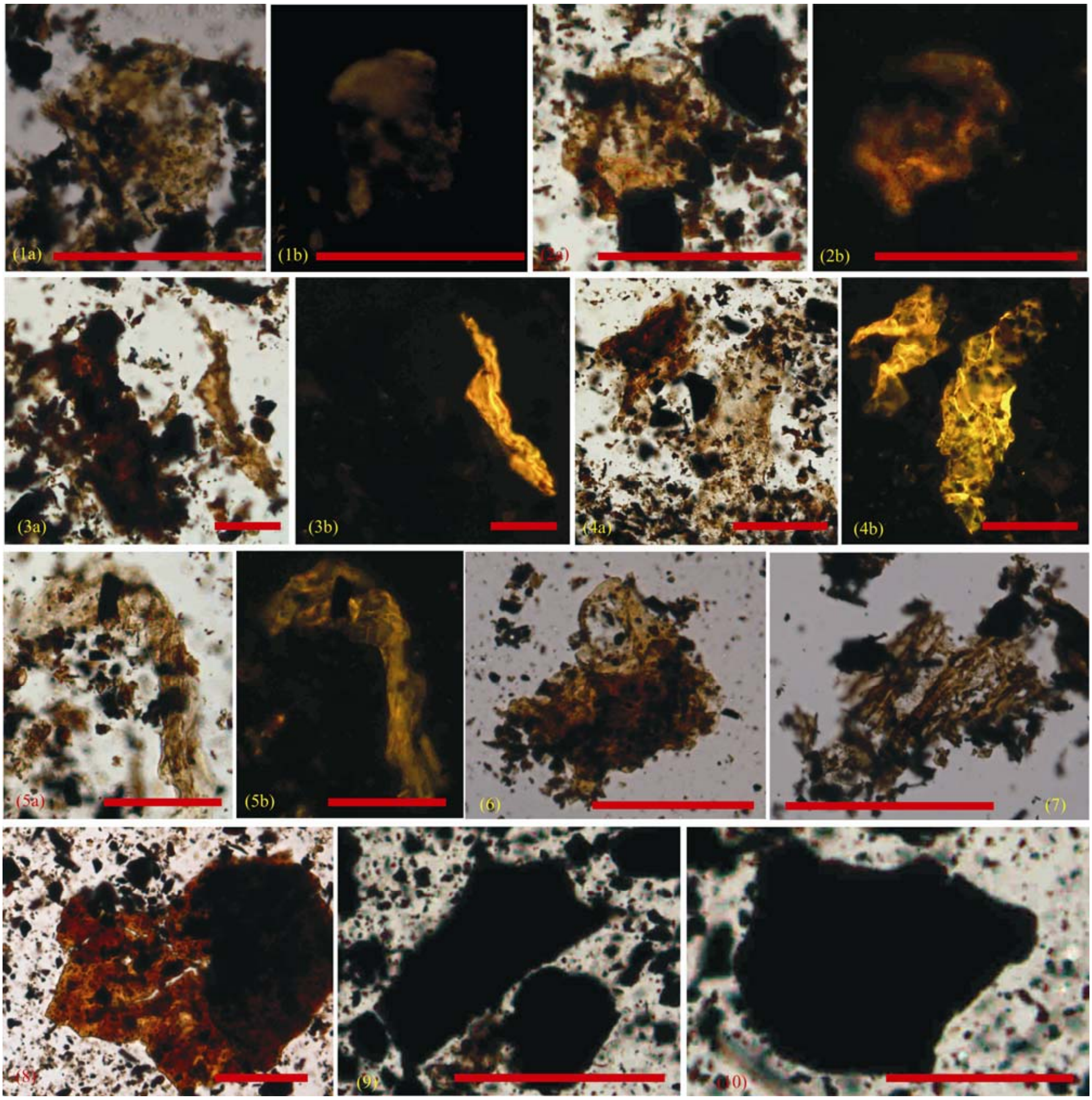

Fig. 6. Photomicrographs of macerals in shale samples under transmitted light and fluorescence (scale=50 μm).
(a), Brown humic AOM show weak fluorescence, (X1-2-10, well X1-2, 1002m); (b), brown humic AOM show moderate fluorescence, (X1-2-32, well X1-2, 1045m); (c), dark brown cutinite show strong fluorescence, (X1-2-20, well X1-2, 873m); (d), brown cutinite show strong fluorescence, (X1-2-17, well X1-2, 920m); (e), brown cutinite show folded structure and moderate fluorescence, (X1-2-17, well X1-2, 920m); (f), dark brown vitrinite with irregular shape, (NP01DH14-4, outcrop, Jungar Banner, Ordos Basin); (g), dark brown vitrinite with original structure of plants (X1-2-20, well X1-2, 873m); (h), reddish brown vitrinite with sharp corners, (BP01DH5-2, outcrop, Jungar Banner, Ordos Basin); (i), black inertinite,(X1-2-32, well X1-2, 1045m); (j), black inertinite, (X1-2-16, well X1-2, 976m).

Blatt, 1984; Gold, 1987; Wilkinson et al., 2001). However, we believe this mechanism maybe subordinate for the Yanan shale because the high feldspar content and smectite/illite content (see below) suggest the dissolution of feldspar is not extensive. In addition, according to the estimation of the silica released by mineral transformation (van de Kamp et al., 2008), the amount of free silica contributed from alteration of feldspar is less comparing to clay mineral transformation，and the free silica generated from clay mineral transforming is more likely to migrate from rather than retain in shale. Therefore, it can be inferred that the mineral transformation leads to loss rather than concentration of silica (van de Kamp et al., 2008).

Smectite illitization is another important reaction in clastic rocks and the illite/smectite is the intermediate product during this progress (Lynch, 1997; van de Kamp,

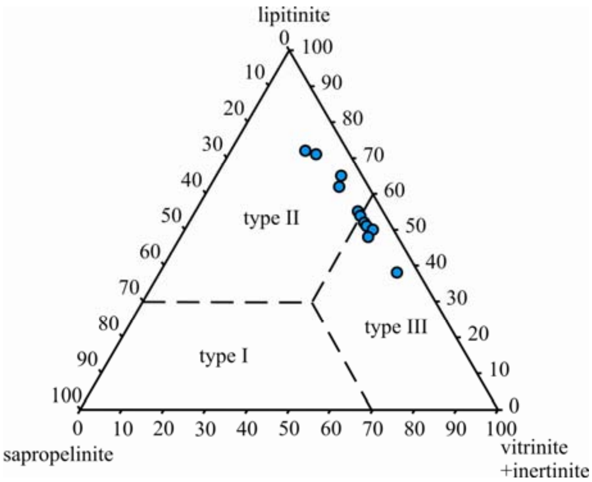

Fig. 7. Organic matter type defined by three terminal graph of maceral composition of shale samples (modified after Hou and Zhang, 2003).

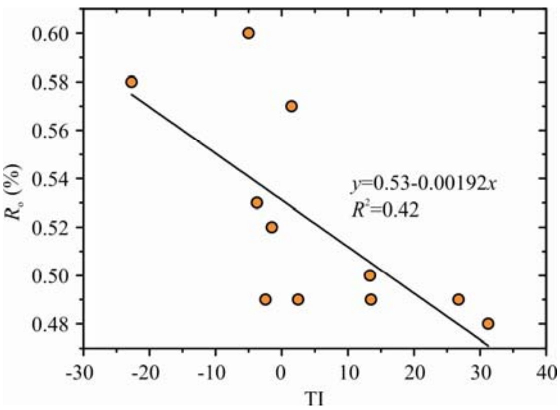

Fig. 8. Negative relationship between R_o and TI of shale samples.

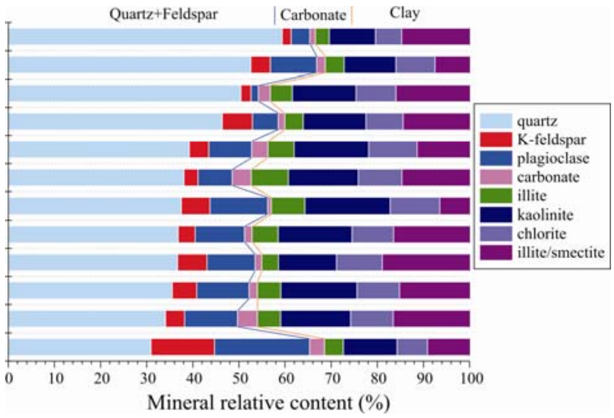

Fig. 9. Mineral composition of shale samples identified by XRD method.

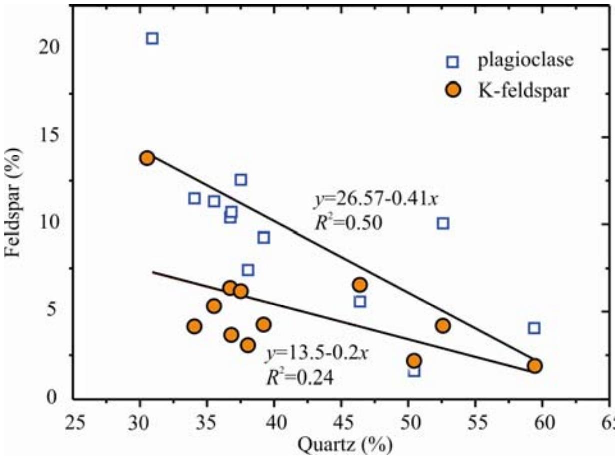

Fig. 10. Plots of quartz content to feldspar content of shale samples.

2008). This reaction takes place over the same temperature (Perry, 1970; Johns and Shimoyama, 1972) interval as hydrocarbon generation and can be enhanced with increasing burial depth (Lynch, 1997). It also requires additional K^+ (Berger et al., 1997), most of which come from the dissolution of K-feldspar (Milliken et al., 1994; Chuhan et al., 2000). In light of the low organic matter maturity as well as the appearance of K-feldspar in the Yanan shale samples, the low illite content and the high content of the intermediate product illite/smectite may suggest smectite-illite transformation is an ongoing process underground, however, the reaction intensity is constrained by the insufficient K^+ and lower temperature.

4.4 Microstructure and pore

Through SEM images, clastic mineral grains, clay mineral aggregates, and organic matter can be distinguished (Fig. 11a). They make up the shale's skeleton between which are tortuous flaky clay and

Table 3 Mineral composition of shale samples

Sample ID	Quartz (%)	Feldspar (%)		Carbonate (%)		Clay (%)			
		K-feldspar	Plagioclase	Dolomite	Siderite	Illite	Kaolinite	Chlorite	Illite/Smectite
X1-2-17	36.73	6.37	10.40	0.00	1.45	3.60	12.62	9.9	18.93
X1-2-15	30.92	13.76	20.63	0.94	2.29	4.09	11.64	6.61	9.12
X1-2-10	34.07	4.15	11.49	0.00	4.28	5.06	15.18	9.20	16.57
X1-2-7	59.40	1.93	4.06	0.00	1.18	3.01	10.03	5.68	14.71
X1-2-26	38.07	3.07	7.40	0.00	4.15	8.04	15.14	9.46	14.67
X1-2-29	37.53	6.18	12.55	0.00	0.74	7.31	18.49	10.75	6.45
X1-2-32	39.22	4.25	9.26	0.00	3.55	5.68	16.17	10.49	11.38
X1-2-35	52.60	4.19	10.06	0.00	1.88	4.07	11.25	8.44	7.51
JX1-1	50.45	2.17	1.59	0.97	1.63	4.75	13.82	8.64	15.98
JX1-3	35.53	5.33	11.32	0.00	1.82	5.06	16.56	9.20	15.18
JX1-4	36.83	3.66	10.71	0.00	1.66	5.66	16.02	8.96	16.50
JX1-6	46.40	6.55	5.58	0.55	0.86	4.0	13.62	8.01	14.43

organic matter paralleling to the bedding. The organic particles are usually with varying shapes and the size of them ranges from several to tens of micrometers (Figs. 11a and b). It has also been observed that small amorphous and isolated organic particles are filled in pore spaces (Fig. 11b). Unlike deep burial shales (Loucks et al., 2012; Chen et al., 2016), the intergranular pores between clastic grains are very common (Fig. 11c). It is also noted that porous mineral aggregates exist in some shelters supported by larger mineral grains (Fig. 11d). This may be a result of loose compaction and suggests that interparticle pores (InterP) in the shale with non-uniform grain size such as the silty and sandy materials have a better chance to survive from pressure.

Compared to marine shale (Loucks et al., 2009; Jiao et al., 2014; Nie Haikuan et al., 2015), the organic matter-hosting pores (OM pores) are much less in the Yanan shale samples at the resolution of SEM. However, though not common, some porous organic matter particles were found in some samples (Figs. 12a, b and c). Nevertheless, these pores are different in shape and size from the immature (Löhr et al., 2015) and mature shales as previous studies have characterized. They are more likely to be polygonal and angular instead of circular-elliptical (Loucks et al., 2009; 2012; Tian et al., 2013). As for size, they mostly range from hundreds of nanometers to several micrometers in diameter which is much larger than general OM mesopore (2–50 nm) in other shales (Loucks et al., 2009, 2012; Milliken et al., 2013; Jiao et al., 2014; Chen et al., 2016). Therefore, instead of hydrocarbon generation (Jarvie et al., 2007), these OM pores may derive from the original intrinsic texture of the organic matter or gelatination and dehydration caused by compaction during early diagenesis (Figs. 12b and c). In addition, some of the OM pores may also be a result of porous clay within the organic matter particles (Figs. 12c and d). Compared with the highly matured marine organic-rich shale, the lack of visible OM pores in the Yanan shale samples probably mainly comes from their lower maturity and predominant type Ⅲ kerogen (Schieber, 2010; Curtis et al., 2012; Bernard et al., 2012; Chen and Xiao, 2014).

Because of the shallower burial depth, the InterP and

Table 4 Pore parameters of shale samples

Sample ID	BET surface area (m^2/g)	BJH pore volume (ml/g)	Average pore diameter (nm)
NP01DH12-1	6.62	0.022	6.72
X1-2-15	5.08	0.015	5.90
X1-2-35	5.06	0.014	5.35
JX1-6	6.86	0.022	6.32
X1-2-17	6.57	0.028	8.38
X1-2-16	5.58	0.019	6.78

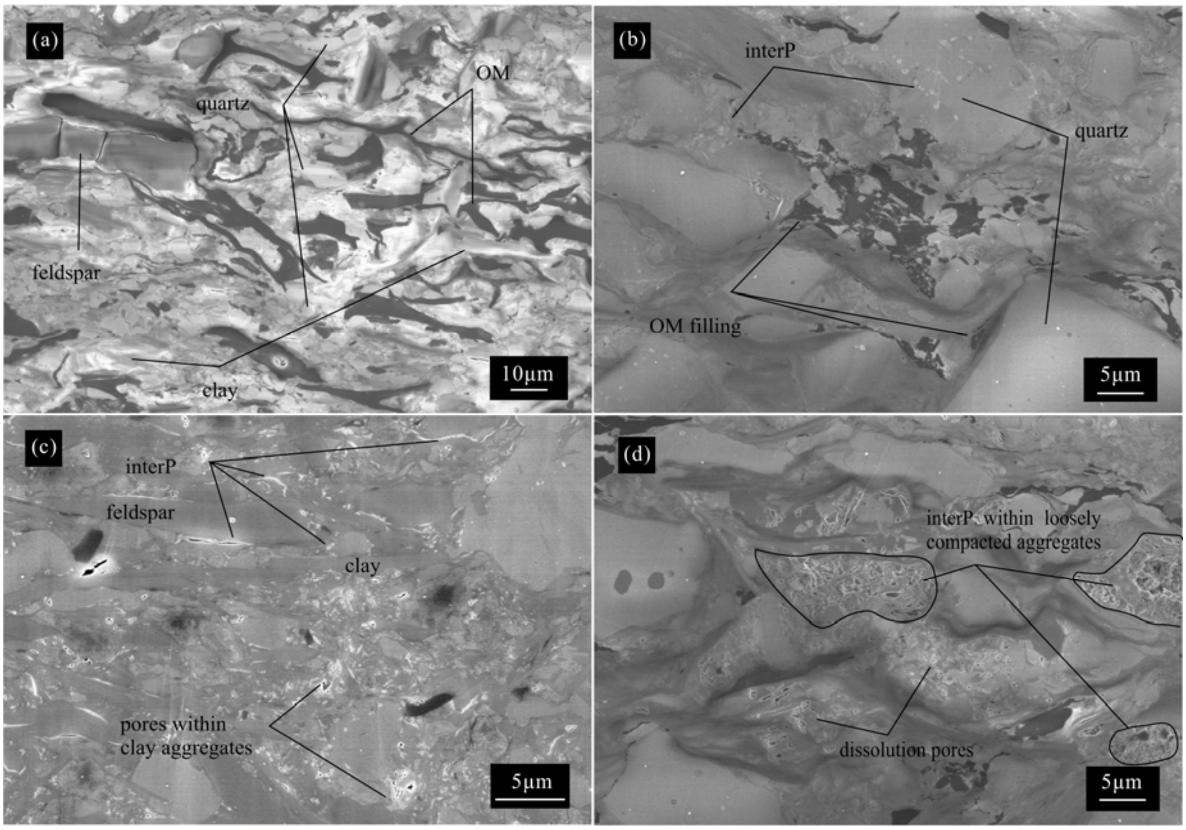

Fig. 11. Bulk microstructure of the Yanan shale samples.
(a), SE image show microstructure, (X1-2-18, well X1-2, 875m); (b), SE image show microstructure, (X1-2-13, well X1-2, 995m); (c), SE image show intergranular pores, (X5-3-22, well X5-3, 911m); (d), SE image show porous mineral aggregates, (X1-2-13, well X1-2, 995m).

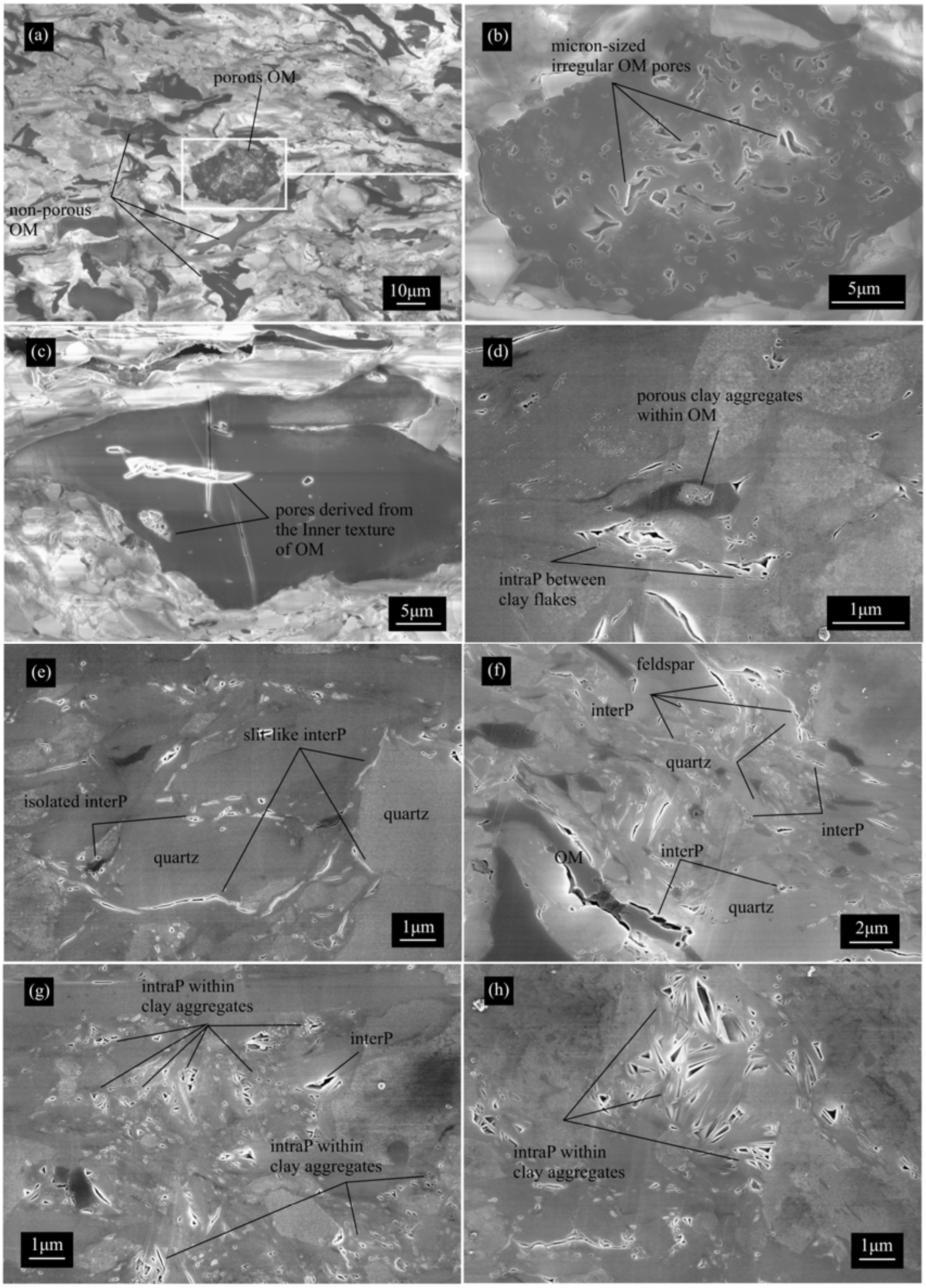

Fig. 12. Pore characteristics of the Yanan shale samples.

(a), SE image show OM pore distribution, (X1-2-18, well X1-2, 875m); (b), SE image show micron-sized irregular OM pores, (X1-2-13, well X1-2, 995m); (c), SE image show isolated OM pores probably derived from the inner texture of OM, (X1-2-18, well X1-2, 875m); (d), SE image show porous clay mineral, (X6-2-21, well X6-2, 983m); (e), SE image show interP between detrital minerals, (X6-2-21, well X6-2, 983m); (F), SE image show developed interP, (X1-2-18, well X1-2, 875m); (g), SE image show intraP within clay aggregates in various shapes, (X1-2-11, well X1-2, 1000m); (h), SE image show intraP within clay aggregates, (X1-2-13, well X1-2, 995m).

intraparticle pores (IntraP) are abundant between clastic grains or within clay aggregates. The interparticle pores occur as either isolated or slit-like pores along the boundary of grains (Figs. 12e and f) depending on the contact with other particles. The intraparticle pores within clay aggregates are recognizable as they are mostly triangle or slit-like in shape (Figs. 12g and h). That is probably a result of stacking of the flaky clay layers (Slatt and O'brien, 2011).

According to the LNA result (Table 3), the BET surface area of the Yanan shale samples ranges from 5.06 to 6.86 m^2/g with an average of 5.96 m^2/g. The BJH pore volume ranges from 0.014 to 0.028 ml/g with an average of 0.20 ml/g. The average diameter of pores between 0.38 nm and 300 nm in diameter (Chalmers et al., 2012) ranges from 5.35 nm to 8.38 nm, and the average value is 6.58 nm. Compared to the Cambrian and Silurian marine shales from Southeast Chongqing and Northwest Guizhou, South China (Wu Jingshu et al., 2013; Han Shuangbiao et al., 2013; Xue Bing et al., 2015; Chen Lei et al., 2017), the Yanan shale samples have lower BET surface area and higher BJH pore volume. The pore size distribution graphs (Fig. 13) demonstrate that although the number of pores decreases with increasing pore size, the contribution of mesopore (2–50nm) and macropore (>50nm) to pore volume is much greater than micropore (<2nm) according to the pore size classification of shale suggested by Chalmers et al., (2012), which has been a consensus for coal measure shale (Pan et al., 2017; Wang Anmin et al., 2017). For the highly matured marine shale, surface area is positively correlated with TOC content, suggesting the high surface area is mainly contributed from the abundant OM micromesopores. When the FE-SEM images and LNA result are combined, it is inferred that the Yanan shale samples have less OM micro-mespores and more macropores than the marine shale.

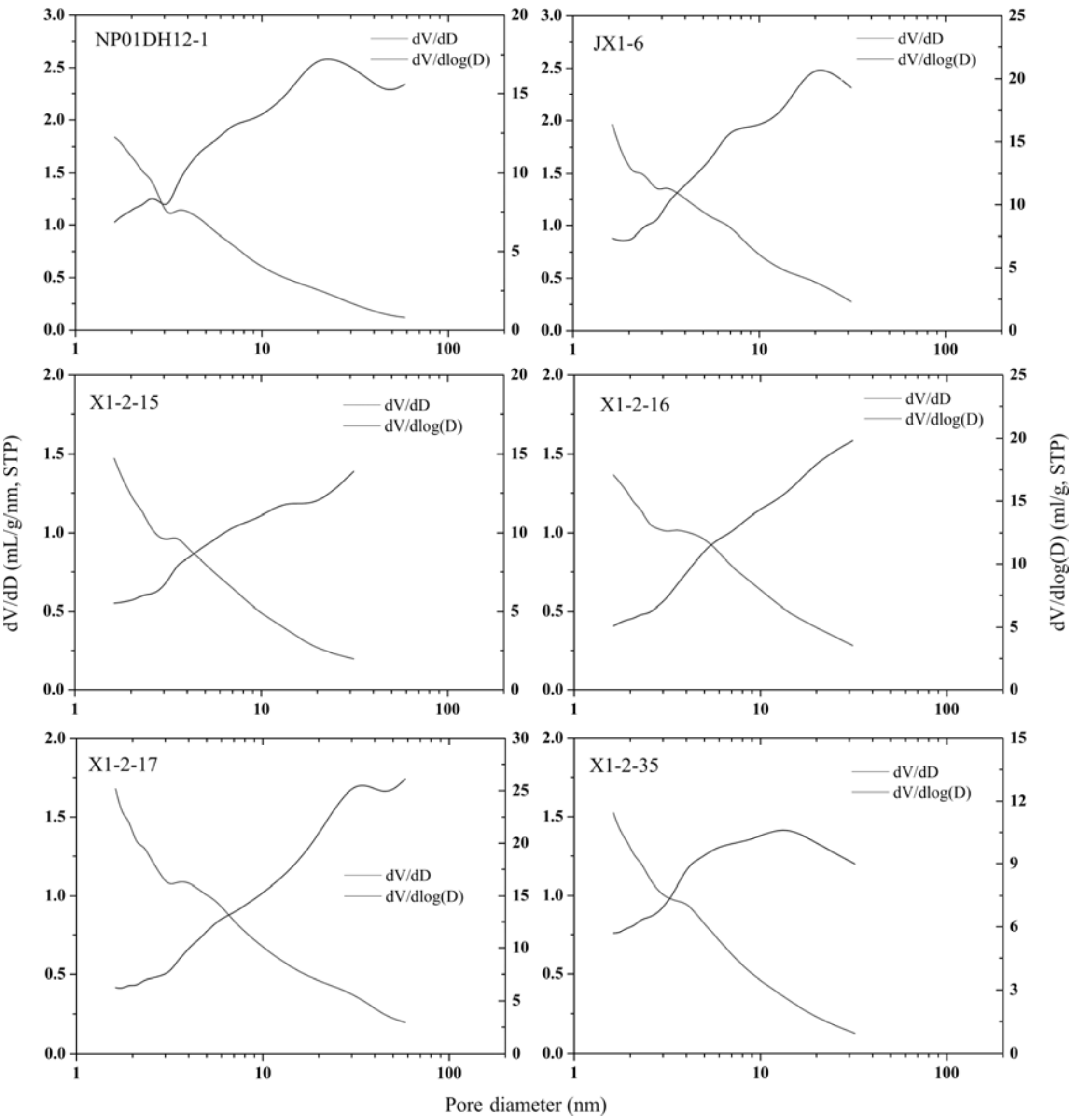

Fig. 13. LNA pore size distribution of shale samples.

5 Discussions

5.1 Evaluation of shale gas reservoir

Theoretically, shale gas is a kind of hydrocarbon accumulation both mostly self-generated and self-stored in the organic-rich shale. For the shale in coal-bearing strata, however, adjacent coal measures can also contribute hydrocarbon to shale reservoir through vertical migration in short distance (Li et al., 2018). In order to achieve economic production, the shale reservoir generally needs to be stimulated to improve permeability by hydraulic fracturing. Therefore, the quality of shale gas reservoir depends mainly on its hydrocarbon generation, storage capacity and how easily the reservoir can be fractured (Feng Dongjun et al., 2016; Wei Xiang feng et al.,2017; Zhang Yuying et al., 2018).

5.1.1 Hydrocarbon generation capacity

According to the organic geochemical analysis, the Yanan shale samples are characterized as organic-rich, early matured shale with predominantly type II_2-III kerogen. According to the microscopic examination of kerogen, continental OM derived from higher plants prevails in the Yanan shale samples. However, humic AMO, as a result of microbial actions, is rich in the samples. This outcome may suggest the original continental OM has been intensively degraded by bacteria, which could improve the quality of parent macerals by increasing hydrogen content. A plate (Fig. 14) based on the relationship between TOC and HI was used to evaluate the quality of shale. It indicates that the samples are mostly fair oil source rocks with several exceptions caused by the samples with TOC less than 1.0%. Generally, the outcrops show either low TOC or low HI values (Figs. 5 and 14) relative to the average level of the core samples, suggesting the OM in the outcrops may be decreased or degraded because of oxidization during weathering (Littke, 1991; Liu et al., 2016; Tang et al., 2017).

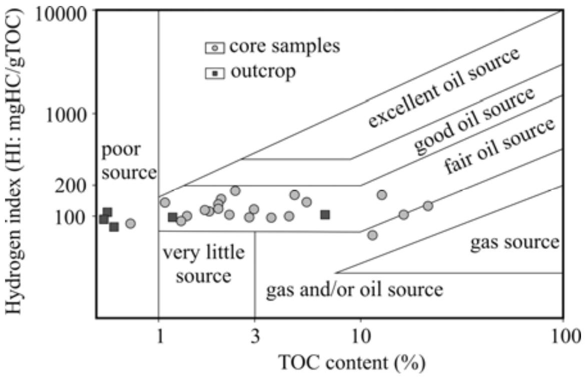

Fig. 14. TOC content versus Hydrogen index (HI) indicates quality of the source rock (modified from Varma et al., 2015).

However, the low production index (PI) (Table 1) indicates the amount of hydrocarbon has been generated was constrained probably by its low thermal maturity. Only two samples with T_{max} above 438°C have a relatively higher PI (Fig. 15). This may suggest the actual extensive thermogenic hydrocarbon generation did not begin for most of the Yanan shales in the study area.

Nevertheless, many previous studies have suggested that biogenetic methane, which can form before the thermogenically-sourced methane, is also a significant component in low-rank coal reservoir (Liu Honglin et al., 2006, 2010; Hamilton et al., 2014; Tang Ying et al., 2017) and can be successfully explored. Sun Bin et al., (2011) have analyzed the carbon isotopes and underground water characteristics of the coalbed methane from Yanan Formation of the Wushen Qi, adjacent to the study area. It was concluded that the methane content of the Yanan coalbed vary from 0.19 m^3/t to 6.7 m^3/t and biogenic gas was proved to be a significant supplement to coalbed methane enrichment in the Yanan Formation in the study area.

5.1.2 Hydrocarbon storage capacity

Shale gas is mainly stored as free gas and adsorption gas. The free gas is compressed in pores like conventional sandstone natural gas while the adsorption gas is mainly adsorbed on organic matter and both internal and external surface of the clay mineral. Previous studies have proved that the methane adsorption capacity of shale can be determined by organic matter richness, clay mineral type and content. Though the surface area is relatively low, the high TOC content and microporous illite/smectite (Ji et al., 2012; Kuila and Prasad, 2013) content are beneficial to methane adsorption capacity of the Yanan shale samples. When using rock density of 2.6g/cm^3, the equivalent porosity of the Yanan shale samples calculated based on BJH pore volume is between 3.64% and 7.28% with an

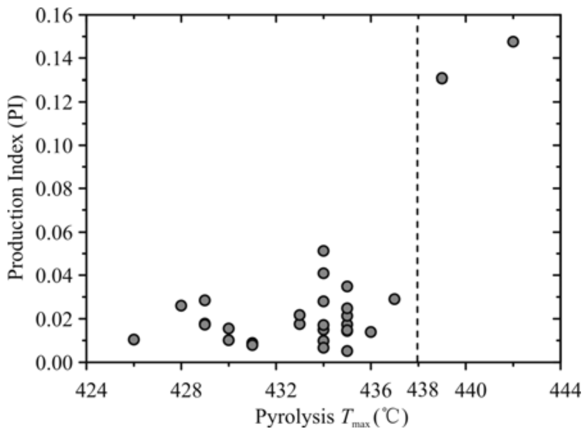

Fig. 15. Pyrolysis T_{max} versus Production index (PI) indicates the efficiency of hydrocarbon generation.

average of 5.2%, and that is comparable to the commercial shale gas reservoir at present. Since the Yanan shale has been less compacted compared to the highly matured Cambrian and Silurian shale in the Sichuan Basin, a certain proportion of micron-sized interP and intraP can be observed through SEM, providing sufficient space for free gas storage. Moreover, larger OM pores in the Yanan shale are probably the reason why the surface area is relatively lower than marine shales and that may lead to a higher proportion of free gas relative to adsorption gas in the Yanan shale.

5.1.3 Brittleness

Brittle mineral content (Bowker, 2007; Jarvie et al., 2007; Yuan Yusong et al., 2017) is an essential parameter to estimate the fracture generation ability of shale under external forces. However, the definition of brittle mineral is still ambiguous and controversial (Rybacki et al., 2016; Zhang et al., 2016; Wang Ruyue et al., 2016). Except for quartz (Kumar et al., 2015; Jarvie et al., 2007), some authors argued that dolomite or total carbonate (Wang and Gale, 2009; Tan et al., 2014) and feldspar (Uffmann et al., 2012; Tan et al., 2014; Guo et al., 2015; Rybacki et al., 2016) should also be recognized as brittle mineral. Sine carbonate is few in the Yanan shale samples, whether feldspar, which accounts for more than 10%, be considered as brittle mineral will significantly influence the evaluation of the brittleness of the samples. If feldspar is included into brittle minerals in this study, the content of brittle minerals of the samples reaches a rather steady level that basically between 50% and 60% (Fig. 9) as there is a negative relationship between quartz and feldspar. And that is almost equivalent to the brittle mineral content of the successful economic gas shales from North America (Chermak and Schreiber, 2014).

5.2 Regional shale gas preservation condition

The three core wells in this study locate at the Yishan slope, which is a steady unicline dipping to the west. After the deposition of Yanan Formation, this area was slightly lifted (Sun Bin et al., 2011). However, no high-angle fractures were observed in core samples (Fig. 2), suggesting the strata was not severely reformed during tectonic actions. According to the three wells, a suite of dark mudstone (10 meters in thickness) widely distributed at the top of Yanan Formation. In addition, above the Yanan Formation, 50 to 100 meters of mudstone existed in the deposition of the Zhiluo Formation (Xue Rui et al., 2017; Lei Kaiyu et al., 2017). The thick overlying mudstone is supposed to act as caprock to prevent shale gas loss from migrating upwardly. When the thickness of shale reaches up to a certain degree, gas can be confined in shale reservoir by its own low porosity and permeability. In the coal-bearing strata, however, thick shale layers are rare because shale is usually frequently interbedded with sandstone, siltstone or coal. In the Yanan Formation, the thickness of shale in a single layer ranges from 0.55 m to 7 m with an average of 3.3 m. Therefore, gas diffusion between shale, coal and sandstone is expected to be common in the coal-bearing strata. It is suggested the whole formation should be considered as an integrated self -storage gas-bearing system, where shale gas, coalbed methane and conventional gas coexist.

6 Conclusions

The terrestrial coal-bearing Yanan Formation in north Ordos Basin has a total thickness of 150–300 m where shale contributes to half of the thickness. In this study, the richness, type and thermal maturity of organic matter, mineralogy, microstructure and pore characteristics of the Yanan shale from north Ordos Basin were analyzed to preliminary evaluate their capacity to be a shale gas reservoir.

(1) The Yanan shale is a suite of fair oil source rock with TOC content ranging from 0.33% to 24.12% and hydrogen index ranging from 43.31mg/g to 330.58 mg/g. Majority of the organic matter-rich samples (TOC>5%) are the carbonaceous shale associated with coal seams. The pyrolysis T_{max} (426–439°C) agrees with the vitrinite reflectance (0.48%–0.60%) and they all suggest the Yanan shale is just at the beginning of oil-generation stage. Humic amorphous organic matter and vitrinite derived from woody plants are the main components of kerogen in the Yanan shale. It suggests most of the OM was altered by bacteria and the organic matter type is Ⅱ–Ⅲ.

(2) The inorganic material in the Yanan shale is mainly composed of quartz, clay and feldspar. Feldspar's content is more than 10%, so whether the feldspar is brittle will significantly influence the brittleness of the Yanan shale. Among the clay minerals, kaolinite, illite/smectite are prevailing while chlorite and illite are less. The quartz content is negatively correlated with feldspar. Higher illite/smectite content and lower illite content suggest the weak smectite illitization probably due to the lower temperature and insufficient K^+ under shallow burial depth.

(3) Because of the lower thermal maturity and dominated woody kerogen, the OM pores in the Yanan shale are less common compared to other matured marine shales. However, some porous organic particles are found and the pores are considered coming from intrinsic structures of the kerogen. Interparticle pores between clastic grains and intraparticle pores associated with clay

mineral are common in the Yanan shale due to a less compaction. The BET Surface area surface ranges from 5.06 to 6.86 m^2/g with an average of 5.96 m^2/g and the BJH pore volume ranges from 0.014 to 0.028 ml/g with an average of 0.20 ml/g. PSD curves suggest the pore volume is more likely to be contributed by macropores.

(4) The Yanan shale is characterized as a suite of low mature fair source rock that possesses good reservoir capacity. The low maturity of the OM constrains the amount of hydrocarbon that can be thermogenically generated. However, knowledge from low-rank coalbed methane development at adjacent areas suggests biogenic gas and coal-derived gas may be a significant supplement to shale gas accumulation in the coal measure formation.

Acknowledgments

Our study is supported by the Ordos administrative district, Ordos Basin shale gas resource potential investigation and evaluation program (grant No. 2013CGKY0893), which was funded by the Ordos city energy investment and development Co., LTD, and the National Natural Science Foundation of China (grant No. 41872124). Thanks are given to Mr. Bai Lingqi, Mr. Lin Haitao and Mr. Feng Yan for their fieldwork.

Manuscript received Apr. 11, 2018
accepted Jul. 27, 2018
edited by Hao Qingqing

References

Andersson, P.O.D., Worden, R.H., Hodgson, D.M., and Flint, S., 2004. Provenance evolution and chemostratigraphy of a Palaeozoic submarine fan-complex: Tanqua Karoo Basin, South Africa. *Marine and Petroleum Geology*, 21: 555–577.

Barrett, E.P., Joyner, L.G., and Halenda, P.P., 1951. The determination of pore volume and area distributions in porous substances. I. Computations from nitrogen isotherms. *Journal of American Chemistry Society*, 73: 373–380.

Behar, F., Beaumont, V., and Penteado, H.L.D., 2001. Rock-Eval 6 technology: performances and developments. *Oil & Gas Science and Technology*, 56: 111–134.

Berger, G., Lacharpagne, J.C., Velde, B., Beaufort, D., and Lanson, B., 1997. Kinetic constrains on illitization reactions and effects of organic diagenesis in sandstone/shale sequences. *Applied Geochemistry*, 12: 23–35.

Bernard, S., Wirth, R., Schreiber, A., Schulz, H.M., and Horsfield, B., 2012. Formation of nanoporous pyrobitumen residues during maturation of the Barnett Shale (Fort Worth Basin). *International Journal of Coal Geology*, 103: 3–11.

Bian Congsheng, Zhao Wenzhi, Wang Hongjun, Chen Zhiyong, Wang Zecheng, Liu Guangdi, Zhao Changyi, Wang Yunpeng, Xu Zhaohui, Li Yongxin and Jiang Lin, 2015. Contribution of moderate overall coal-bearing basin uplift to tight sand gas accumulation: case study of the Xujiahe Formation in the Sichuan Basin and the Upper Paleozoic in the Ordos Basin, China. *Petroleum Science*, 12: 218–231.

Bowker, K.A., 2007. Barnett Shale gas production, Fort Worth Basin: issues and discussion. *American Association of Petroleum Geologists Bulletin*, 91: 523–533.

Brunauer, S., Deming, L.S., Deming, W.E., and Teller, E., 1940. On a theory of the van der waals adsorption of gases. *Journal of American Chemistry Society*, 62: 1723–1732.

Cao Qingying, 1985. Identification of microcomponents and types kerogen under transmitted light. *Petroleum Exploration and Development*, 5: 14–23 (in Chinese with English abstract).

Chalmers, G.R., Bustin, R.M., and Power, I.M., 2012. Characterization of gas shale pore systems by porosimetry, pycnometry, surface area, and field emission scanning electron microscopy/transmission electron microscopy image analyses: examples from the Barnett, Woodford, Haynesville, Marcellus, and Doig unit. *AAPG Bulletin*, 96(6): 1099–1119.

Chen Lei, Jiang Zhenxue, Liu Keyu, Gao Fenglin and Wang Pengfei, 2017. A combination of N_2 and CO_2 adsorption to characterize nanopore structure of organic-rich lower Silurian shale in the upper Yangtze platform, South China: implications for shale gas sorption capacity. *Acta Geologica Sinica* (English Edition), 91: 1380–1394.

Chen, J., and Xiao, X., 2014. Evolution of nanoporosity in organic-rich shales during thermal maturation. *Fuel*, 129: 173–181.

Chen, Q., Zhang, J., Tang, X., Li, W., and Li, Z., 2016. Relationship between pore type and pore size of marine shale: an example from the Sinian–Cambrian Formation, upper Yangtze region, South China. *International Journal of Coal Geology*, 158: 13–28.

Chermak, J.A., and Schreiber, M.E., 2014. Mineralogy and trace element geochemistry of gas shales in the United States: environmental implications. *International Journal of Coal Geology*, 126: 32–44.

Chuhan, F.A., Bjørlykke, K., and Lowrey, C., 2000. The role of provenance in illitization of deeply buried reservoir sandstones from Haltenbanken and north Viking Graben, offshore Norway. *Marine and Petroleum Geology*, 17: 673–689.

Curtis, M.E., Cardott, B.J., Sondergeld, C.H., and Rai, C.S., 2012. Development of organic porosity in the Woodford Shale with increasing thermal maturity. *International Journal of Coal Geology*, 103: 26–31.

Dang, W., Zhang, J., Tang, X., Chen, Q., Han, S., Li, Z., Du, X., Wei, X., Zhang, M., Liu, J., Peng, J., and Huang, Z., 2016. Shale gas potential of Lower Permian marine-continental transitional black shales in the Southern north china basin, central China: characterization of organic geochemistry. *Journal of Natural Gas Science and Engineering*, 28: 639–650.

Feng Dongjun, Hu Zongquan, Gao Bo, Peng Yongmin and Du Wei, 2016. Analysis of shale gas reservoir-forming condition of Wufeng Formation-Longmaxi Formation in southeast Sichuan Basin. *Geological Review*, 62(6): 1521–1532 (in Chinese with English abstract).

Feng Sanli, 2002. Coalbed methane resources in the Ordos Basin and its development potential. *Geological Bulletin of China*, 21: 658–662 (in Chinese with English abstract).

Gold, P.B., 1987. Textures and geochemistry of authigenic albite from Miocene sandstones, Louisiana Gulf Coast. *Journal of*

Sedimentary Petrology, 57: 353–362.

Guan, Q., Dong, D., Wang, S., Huang, J., Wang, Y., Lu, H., and Zhang, C., 2016. Preliminary study on shale gas microreservoir characteristics of the Lower Silurian Longmaxi Formation in the southern Sichuan Basin, China. *Journal of Natural Gas Science and Engineering*, 31: 382–395.

Guo, T., Zhang, S., Ge, H., Wang, X., Lei, X., and Xiao, B., 2015. A new method for evaluation of fracture network formation capacity of rock. *Fuel*, 140: 778–787.

Gupta, N., Rai, C.S., and Sondergeld, C.H., 2013. Petrophysical characterization of the Woodford Shale. *Petrophysics*, 54: 368–382.

Hamilton, S.K., Golding, S.D., Baublys, K.A., and Esterle, J.S., 2014. Stable isotopic and molecular composition of desorbed coal seam gases from the Walloon subgroup, eastern Surat Basin, Australia. *International Journal of Coal Geology*, 122: 21–36.

Han Shuangbiao, Zhang Jinchuan, Yang Chao, Lin Lamei, Zhu Liangliang, Chen Yongchang and Xue Bing, 2013. The characteristics of nanoscale pore and its gas storage capability in the Lower Cambrian shale of southeast Chongqing. *Journal of China Coal Society*, 38(6):1038–1043 (in Chinese with English abstract).

Han Zongyuan, Miao Jianyu and Bu Zhanqi, 2007. The comparative study on organic geochemical characters of Mesozoic source rocks in T_3y and J_2Y of Zhenyuan in Ordos Basin. *Geoscience*, 21: 532–537 (in Chinese with English abstract).

Hanson, A.D., Ritts, B.D., and Moldowan, J.M., 2007. Organic geochemistry of oil and source rock strata of the Ordos Basin, north-central China. *AAPG Bulletin*, 91: 1273–1293.

Hao F., and Chen J., 2010. The cause and mechanism of vitrinite reflectance anomalies. *Journal of Petroleum Geology*, 15: 419–434.

Hao Ziguo, Fei Hongcai, Hao Qingqing and Liu Lian., 2017. China's shale gas geological investigation and prospecting have made significant progress. *Acta Geologica Sinica* (English Edition), 91: 727–728.

He Zixin, Fu Jinhua, Xi Shengli, Fu Suotang and Bao Hongping, 2003. Geological features of reservoir formation of Sulige gas field. *Acta Petrolei Sinica*, 24: 6–12 (in Chinese with English abstract).

Heller, R., and Zoback, M., 2014. Adsorption of methane and carbon dioxide on gas shale and pure mineral samples. *Journal of Unconventional Oil and Gas Resources*, 8: 14–24.

Hou Dujie and Zhang Linye, 2003. *Oil and Gas Geochemical Plates*. Beijing: Petroleum Industry Press (in Chinese).

Huang Gang, Zhou Xiqiang and Wang Zhengquan, 2009. Provenance analysis of the Yan'an Formation in Mid-Jurassic at the southeast area of Ordos Basin. *Bulletin of Mineralogy Petrology and Geochemistry*, 28: 252–258 (in Chinese with English abstract).

Huang Wenhui, Ao Weihua, Weng Chengmin, Xiao Xiuling, Liu Dameng, Tang Xiuyi, Chen Ping, Zhao Zhigen, Wan Huan and Finkelman, B., 2010. Characteristics of coal petrology and genesis of Jurassic coal in Ordos Basin. *Geoscience*, 24: 1186–1197 (in Chinese with English abstract).

Huang Wenhui, Ao Weihua, Xiao Xiuling and Wan Huan, 2011. The assesment of the capacity for producing hadrocarbon in the Jurrasic coal and associate rocks in Ordos Basin. *Journal of China Coal Society*, 36: 461–467 (in Chinese with English abstract).

Hutton, A.C., and Cook, A.C., 1980. Influence of alginite on the reflectance of vitrinite from Joadja, NSW, and some other coals and oil shales containing alginite. *Fuel*, 59: 711–714.

Jarvie, D.M., Hill, R.J., Ruble, T.E., and Pollastro, R.M., 2007. Unconventional shale–gas systems: the Mississippian Barnett Shale of north–central Texas as one model for thermogenic shale-gas assessment. *AAPG Bulletin*, 91: 475–499.

Ji, L., Zhang, T., Milliken, K.L., Qu, J., and Zhang, X., 2012. Experimental investigation of main controls to methane adsorption in clay-rich rocks. *Applied Geochemistry*, 27: 2533–2545.

Ji, W., Song, Y., Jiang, Z., Wang, X., Bai, Y., and Xing, J., 2014. Geological controls and estimation algorithms of lacustrine shale gas adsorption capacity: a case study of the Triassic strata in the southeastern Ordos Basin, China. *International Journal of Coal Geology*, 134–135: 61–73.

Jiang, S., Xu, Z., Feng, Y., Zhang, J., Cai, D., Chen, L., Wu, Y., Zhou, D., Bao, S., and Long, S., 2016. Geologic characteristics of hydrocarbon-bearing marine, transitional and lacustrine shales in China. *Journal of Asian Earth Sciences*, 115: 404–418.

Jiang, Z., Xu, J., and Wang, G., 2012. The discovery and significance of a sedimentary hiatus within the Carboniferous Taiyuan Formation, northeastern Ordos Basin, China. *AAPG Bulletin*, 96: 1173–1195.

Jiao, K., Yao, S., Liu, C., Gao, Y., Wu, H., Li, M., and Tang, Z., 2014. The characterization and quantitative analysis of nanopores in unconventional gas reservoirs utilizing FESEM–FIB and image processing: an example from the Lower Silurian Longmaxi Shale, upper Yangtze region, China. *International Journal of Coal Geology*, 128–129: 1–11.

Johns, W.D., and Shimoyama, A., 1972. Clay minerals and petroleum-forming reactions during burial and diagenesis. *American Association of Petroleum Geologists Bulletin*, 56:11: 2160–2167.

Jones, R.L., and Blatt, H., 1984. Mineral dispersal patterns in the Pierre Shale. *Journal of Sedimentary Research*, 54: 17–28.

Kalkreuth, W.D., 1982. Rank and petrographic composition of selected Jurassic-Lower Cretaceous coals of British Columbia, Canada. *Bulletin of Canadian Petroleum Geology*, 30: 112–139.

Kuhn, G., and Diekmann, B., 2002. Late Quaternary variability of ocean circulation in the southeastern South Atlantic inferred from the terrigenous sediment record of a drift deposit in the southern Cape Basin (ODP Site 1089). *Palaeogeography Palaeoclimatology Palaeoecology*, 182: 287–303.

Kuila, U., and Prasad, M., 2013. Specific surface area and pore-size distribution in clays and shales. *Geophysical Prospecting*, 61: 341–362.

Kumar, V., Sondergeld, C., and Rai, C.S., 2015. Effect of mineralogy and organic matter on mechanical properties of shale. *Interpretation*, 3: SV9–SV15.

Lei Kaiyu, Liu Chiyang, Zhang Long, Wu Bolin, Cun Xiaoni and Sun Li, 2017. Element geochemical characteristics of the Jurassic mudstones in the northern Ordos Basin: implications for tracing sediment sources and paleoenvironment restoration. *Acta Sedimentologica Sinica*, 35: 621–636 (in Chinese with English abstract).

Li Ping, Li Shengfu, Liu Yu, Yin Song, Fu Duowang and Yang

Xiaoqiang, 2018. Reservoir models of the coal measure shale gas in the Qinshui Basin. *Geology and Exploration*, 54: 395–403 (in Chinese with English abstract).

Li Zixue, Shao Long Yi, Li Mingpei and Chen Fei, 2014. Analysis of shale gas resource exploration potential of Yan'an Formation in northern Huangling mining area of Ordos Basin. *Coal Geology & Exploration*, 42: 31–35 (in Chinese with English abstract).

Littke, R., Klussmann, U., Krooss, B., and Leythaeuser, D., 1991. Quantification of loss of calcite, pyrite, and organic matter due to weathering of Toarcian black shales and effects on kerogen and bitumen characteristics. *Geochimica et Cosmochimica Acta*, 55, 3369–3378.

Liu Honglin, Li Guizhong, Wang Hongyan, Yang Yong, Wang Bo and Liu Ping, 2006. Study on simulation of biogenic coalbed methane in the low coal rank basin northwestern China. *Petroleum Geology and Experiment*, 28: 600–603 (in Chinese with English abstract).

Liu Honglin, Wang Hongyan, Zhao Qun, Liu Yingji, Sang Shuxun and Yong Hong, 2010. Geological characteristics of coalbed methane and controlling factors of accumulation in the Tuha coal basin. *Acta Geologica Sinica*, 84: 133–137 (in Chinese with English abstract).

Liu, G., Huang, Z., Chen, F., Jiang, Z., Gao, X., Li, T., Chen, L., Xia, L., and Han, W., 2016. Reservoir characterization of Chang 7 member shale: a case study of lacustrine shale in the Yanchang Formation, Ordos Basin, China. *Journal of Natural Gas Science and Engineering*, 34: 458–471.

Liu, Y., Zhang, J., Tang, X., Yang, C., and Tang, S., 2016. Weathering characteristics of the Lower Paleozoic black shale in northwestern Guizhou Province, south China. *Journal of Earth System Science*, 125: 1–18.

Lo, H.B., 1993. Correction criteria for the suppression of vitrinite reflectance in hydrogen-rich kerogens: preliminary guidelines. *Organic Geochemistry*, 20: 653–657.

Löhr, S.C., Baruch, E.T., Hall, P.A., and Kennedy, M.J., 2015. Is organic pore development in gas shales influenced by the primary porosity and structure of thermally immature organic matter? *Organic Geochemistry*, 87: 119–132.

Loucks, R.G., Reed, R.M., Ruppel, S.C., and Hammes, U., 2012. Spectrum of pore types and networks in mudrocks and a descriptive classification for matrix-related mudrock pores. *AAPG Bulletin*, 96: 1071–1098.

Loucks, R.G., Reed, R.M., Ruppel, S.C., and Jarvie, D.M., 2009. Morphology, genesis, and distribution of nanometer-scale pores in siliceous mudstones of the Mississippian Barnett shale. *Journal of Sedimentary Research*, 79: 848–861.

Lynch, F.L., 1997. Frio shale mineralogy and the stoichiometry of the smectite-to-illite reaction: the most important reaction in clastic sedimentary diagenesis. *Clays and Clay Minerals*, 45: 618–631.

Makeen, Y.M., Abdullah, W.H., Hakimi, M.H., and Mustapha, K.A., 2015. Source rock characteristics of the Lower Cretaceous Abu Gabra Formation in the Muglad Basin, Sudan, and its relevance to oil generation studies. *Marine and Petroleum Geology*, 59: 505–516.

Miao Jianyu, Zhao Jianyu, Li Wenhou, Han Zongyuan and Ma Jing, 2005. Reseach on the diposite environments about source rocks in south Ordos Basin. *Journal of Northwest University* (Natural Science Edition), 35: 771–776 (in Chinese with English abstract).

Milliken, K.L., Mack, L.E., and Land, L.S., 1994. Elemental mobility in sandstones during burial; whole-rock chemical and isotopic data, Frio Formation, South Texas. Journal of Sedimentary Research, Section A: *Sedimentary Petrology and Processes; (United States)*, 64:4: 788–796.

Milliken, K.L., Rudnicki, M., Awwiller, D.N., and Zhang, T., 2013. Organic matter-hosted pore system, Marcellus Formation (Devonian), Pennsylvania. *AAPG Bulletin*, 97: 177–200.

Nicolás-López, R., and Valdiviezo-Mijangos, O.C., 2016. Rock physics templates for integrated analysis of shales considering their mineralogy, organic matter and pore fluids. *Journal of Petroleum Science and Engineering*, 137: 33–41.

Nie Haikuan and Jin Zhijun, 2016. Source rock and cap rock controls on the upper Ordovician Wufeng Formation-lower Silurian Longmaxi Formation shale gas accumulation in the Sichuan Basin and its peripheral areas. *Acta Geologica Sinica* (English Edition), 90: 1059–1060.

Nie Haikuan, Zhang Jinchuan and Jiang Shu, 2015. Types and characteristics of the Lower Silurian shale gas reservoirs in and around the Sichuan Basin. *Acta Geologica Sinica* (English Edition), 89: 1973–1985.

Pan, J., Peng C., Wan X., Zheng D., Lv, R., and Wang K., 2017. Pore structure characteristics of coal-bearing organic shale in Yuzhou coalfield, China using low pressure N_2, adsorption and FE-SEM methods. *Journal of Petroleum Science and Engineering*, 153: 234–243.

Perry, E., 1970. Burial diagenesis in Gulf Coast pelitic sediments. *Clays and Clay Minerals*, 18: 165–177.

Pettijohn E.J., 1975. *Sedimentary rocks, 3rd edition*. Harper and Row, New York.

Price, L.C., and Baker, C.E., 1985. Suppression of vitrinite reflectance in amorphous rich kerogen-a major unrecognized problem. *Journal of Petroleum Geology*, 8: 59–84.

Raymond, A.C., and Murchison, D.G., 1991. Influence of exinite macerals on the reflectance of Carboniferous sediments of the Midland Valley of Scotland. *Fuel*, 70: 155–161.

Rybacki, E., Meier, T., and Dresen, G., 2016. What controls the mechanical properties of shale rocks? – Part II: Brittleness. *Journal of Petroleum Science and Engineering*, 144: 39–58.

Schieber, J., 2010. Common themes in the formation and preservation of intrinsic porosity in shales and mudstones – illustrated with examples across the Phanerozoic. SPE-132370, SPE Unconventional Gas Conference. February 23–25, 2010, Pittsburgh, PA.

Schmoker, J.W., 2002. Resource-assessment perspectives for unconventional gas systems. *AAPG Bulletin*, 86: 1993–1999.

Shao Longyi, Hou Haihai, Tang Yue, Lu Jing, Qiu Haijun, Wang Xuetian and Zhang Jiaqiang, 2015. Selection of strategic relay areas of CBM explorationand development in China. *Natural Gas Industry*, 35: 1–11 (in Chinese with English abstract).

Slatt, R.M., and O'Brien, N.R., 2011. Pore types in the Barnett and Woodford gas shales: contribution to understanding gas storage and migration pathways in fine-grained rocks. *AAPG Bulletin*, 95: 2017–2030.

Sone, H., and Zoback, M.D., 2013. Mechanical properties of shale-gas reservoir rocks—Part 1: static and dynamic elastic properties and anisotropy. *Geophysics*, 78: 381–D392.

Sun Bin, Sun Fenjin, Tian Wenguang, Sun Qinping, Chen Gang, Chen Hao and Feng Sheng, 2011. Controlling factors of coalbed methane enrichment in the Wushenqi area, Ordos

Basin. *Natural Gas Industry*, 31: 34–38 (in Chinese with English abstract).

Tan, J., Horsfield, B., Fink, R., Krooss, B., Schulz, H.M., Rybacki, E., Zhang, J., Boreham, C.J., van Graas, G., and Tocher, B.A., 2014. Shale gas potential of the major marine shale formations in the upper Yangtze Platform, South China, Part III: mineralogical, lithofacial, petrophysical, and rock mechanical properties. *Energy and Fuels*, 28: 2322–2342.

Tan, J., Weniger, P., Krooss, B., Merkel, A., Horsfield, B., Zhang, J., Boreham, C.J., van Graas, G., and Tocher, B.A., 2014. Shale gas potential of the major marine shale formations in the upper Yangtze platform, South China, Part II: Methane sorption capacity. *Fuel*, 129: 204–218.

Tang Shuheng, Sun Shenglin, Hao Duohu and Tang Dazhen, 2004. Coalbed methane-bearing characteristics and reservoir physical properties of principal target areas in North China. *Acta Geologica Sinica* (English Edition), 78: 724–728.

Tang Xuan, Zhang Jinchuan, Shan Yansheng and Xiong Jinyu, 2012. Upper Paleozoic coal measures and unconventional natural gas systems of the Ordos Basin, China. *Geoscience Frontiers* (English Edition), 3: 863–873.

Tang Ying, Gu Feng, Wu Xiaodan, Ye Hao, Yu Yixin and Zhong Mihong, 2017. Coalbed methane accumulation conditions and enrichment models of Walloon coal measure in the Surat Basin, Australia. *Natural Gas Industry*, 37: 18–28 (in Chinese with English abstract).

Tang Ying, Li Lezhong, Su Zhan and Wu Xiaodan, 2016. Inhibition of vitrinite reflectance of shale and its correction: a case study on Toolebuc shale of Galilee Basin in Australia. *Journal of Xi'an Shiyou University* (Natural Science Edition), 31: 17–22 (in Chinese with English abstract).

Tang, X., Zhang, J., Liu, Y., Yang, C., Chen, Q., Dang, W., and Zhao, P., 2017. Geochemistry of organic matter and elements of black shale during weathering in northern Guizhou, southwestern China: their mobilization and inter-connection. *Chemie der Erde – Geochemistry*, 78: 140–151.

Tang, X., Zhang, J., Wang, X., Yu, B., Ding, W., Xiong, J., Yang, Y., Wang, L., Yang, C., 2014. Shale characteristics in the southeastern Ordos Basin, China: implications for hydrocarbon accumulation conditions and the potential of continental shales. *International Journal of Coal Geology*, 128–129: 32–46.

Tian, H., Pan, L., Xiao, X., Wilkins, R.W.T., Meng, Z., and Huang, B., 2013. A preliminary study on the pore characterization of Lower Silurian black shales in the Chuandong Thrust Fold Belt, southwestern China using low pressure N_2 adsorption and FE-SEM methods. *Marine and Petroleum Geology*, 48: 8–19.

Uffmann, A.K., Littke, R., and Rippen, D., 2012. Mineralogy and geochemistry of Mississippian and Lower Pennsylvanian black shales at the northern margin of the Variscan mountain belt (Germany and Belgium). *International Journal of Coal Geology*, 103: 92–108.

van de Kamp, P.C., 2008. Smectite-illite-muscovite transformations, quartz dissolution, and silica release in shales. *Clay and Clay Mineral*, 56: 66–81.

Varma, A.K., Hazra, B., Mendhe, V.A., Chinara, I., and Dayal, A.M., 2015. Assessment of organic richness and hydrocarbon generation potential of Raniganj Basin shales, West Bengal, India. *Marine and Petroleum Geology*, 59: 480–490.

Wang Anmin, Cao Daiyong, Li Jing, Jiang Ailin and Yang Chengwei, 2017. A new discovery on the deformation behavior of shale gas reservoirs affecting pore morphology in the Juhugeng coal mining area of Qinghai Province, Northwest China. *Acta Geologica Sinica* (English Edition), 91: 1932–1933.

Wang Ruyue, Gong Dajian, Ding Wenlong, Leng Jigao, Yin Shuai, Wang Xinghua and Sun Yaxiong, 2016. Brittleness evaluation of the lower Cambrian Niutitang shale in the upper Yangtze region: a case study in the Cengong block, Guizhou Province. *Earth Science Frontiers*, 23: 87–95 (in Chinese with English abstract).

Wang Shejiao, Li Denghua, Li Jianzhong, Dong Dazhong, Zhang Wenzheng and Ma Jun, 2011. Exploration potential of shale gas in the Ordos Basin. *Natural Gas Industry*, 31: 40–46 (in Chinese with English abstract).

Wang Xiangzeng, Gao Shengli and Gao Chao, 2014. Geological features of Mesozoic lacustrine shale gas in south of Ordos Basin, NW China. *Petroleum Exploration and Development*, 41: 326–337.

Wang, F.P., and Gale, J.F.W., 2009. Screening criteria for shale-gas systems. *Gulf Coast Association of Geological Societies Transactions*, 59: 779–793.

Wei Xiangfeng, Zhao Zhengbao, Wang Qingbo, Liu Zhujiang, Zhou Min and Zhang Hui, 2017. Comprehensive evaluation on geological conditions of the shale gas in Upper Ordovician Wufeng Formation-Lower Silurian Longmaxi Formation in Dingshan area, Qijiang, southeastern Sichuan. *Geological Review*, 63(1):153–164 (in Chinese with English abstract).

Wilkinson, M., Milliken, K.L., and Haszeldine, R.S., 2001. Systematic destruction of K-feldspar in deeply buried rift and passive margin sandstones. *Journal of the Geological Society*, 158: 675–683.

Wu Jingshu, Yu Bingsong and Zhang Jinchuan, 2013. Pore characteristics and controlling factors in the organic-rich shale of the lower Silurian Longmaxi Formation revealed by samples from a well in southeastern Chongqing. *Earth Science Frontiers*, 20: 260–269 (in Chinese with English abstract).

Wüst, R.A.J., 2013. Vitrinite reflectance versus pyrolysis *T*max data: assessing thermal maturity in shale plays with special reference to the Duvernay shale play of the Western Canadian Sedimentary Basin, Alberta, Canada. *Spe Journal* 167031-MS.

Xiao, X.M., Zhao, B.Q., Thu, Z.L., Song, Z.G., and Wilkins, R.W.T., 2005. Upper Paleozoic petroleum system, Ordos Basin, China. *Marine and Petroleum Geology*, 22: 945–963.

Xie Mingju, and Qiu Nansheng, 2005. Inorganic geochemical explanation of abnormal vitrinitere flectance: taking Niu-38 well in Dongying sag, Jiyang depression as an example. *Journal of Xi'an Shiyou University* (Natural Science Edition), 20: 12–16 (in Chinese with English abstract).

Xue Bing, Zhang Jinchuan, Tang Xuan, Yang Chao, Chen Qian, Man Xiangjie and Dang Wei, 2015. Characteristics of microscopic pore and gas accumulation on shale in Longmaxi Formation, northwest Guizhou. *Acta Petrolei Sinica*, 36(2): 138–149 and 173 (in Chinese with English abstract).

Xue Rui, Zhao Junfeng, Yan Zhandong, Yang Yao, Zhao Xudong and Zhao Zhongping. 2017. Sedimentary characteristics and evolution of the Jurassic Zhiluo Formation in northern Ordos Basin. *Journal of Palaeogeography*, 19: 999–1012 (in Chinese with English abstract).

Yang, Y., Li, W., and Ma, L., 2005. Tectonic and stratigraphic controls of hydrocarbon systems in the Ordos Basin: A multicycle cratonic basin in central China. *AAPG Bulletin*, 89: 255–269.

Yang, Y., Liang, C., Zhang, J., Jiang, Z., and Tang, X., 2015. A developmental model of lacustrine shale gas genesis: A case from T_3y^7 shale in the Ordos Basin, China. *Journal of Natural Gas Science and Engineering*, 22: 395–405.

Yuan Yusong, Jin Zhijun, Zhou Yan, Liu Junxin, Li Shuangjian and Liu Quanyou, 2017. Burial depth interval of the shale brittle-ductile transition zone and its implications in shale gas exploration and production. *Petroleum Science*, 14(4): 637–647.

Zhang Jinchuan, Xu Bo, Nie Haikuan and Deng Feiyong, 2007. Two essential gas accumulations for natural gas exploration in China. *Natural Gas Industry*, 27: 1–6 (in Chinese with English abstract).

Zhang Jinchuan, Yang Chao, Chen Qian, Zhao Qianru, Wei Pengfei and Jiang Shengling, 2016. Deposition and distribution of potential shales in China. *Earth Science Frontiers*, 23: 74–86 (in Chinese with English abstract).

Zhang Juan, 2017. Maturity determination of hydrocarbon source rocks in Xihu dag: evidence from fluorescence alteration of multiple macerals. *Petroleum Geology and Experiment*, 39: 417–422 (in Chinese with English abstract).

Zhang Peihe, 2007. Coalbed methane (CBM) development potential of low rank coal: a case study from Ordos Basin. *Coal Geology and Exploration*, 35: 29–33 (in Chinese with English abstract).

Zhang Yongsheng, Zheng Mianping, Xing Enyuan, Li Yangchi, Gui Baoling, Shi Lizhi, He Yongtao, Wang Linlin, Peng Yuan and Zhao Haitong, 2017. Discovery of marine-terrestrial transitional facies shale gas in Taiyuan Formation of Zhenjia 1 well, northern Shaanxi, Ordos Basin. *Acta Geologica Sinica* (English Edition), 91:1141–1142.

Zhang Yuying, He Zhiliang, Jiang Shu, Lu Shuangfang, Xiao Dianshi, Chen Guohui and Zhao Jianhua, 2018. Controls on the organic carbon content of the lower Cambrian black shale in the southeastern margin of Upper Yangtze.*Petroleum Science*, 15(4): 709–721.

Zhang, D., Ranjith, P.G., and Perera, M.S.A., 2016. The brittleness indices used in rock mechanics and their application in shale hydraulic fracturing: s review. *Journal of Petroleum Science and Engineering*, 143: 158–170.

Zhang, Z., Sun, K., and Yin, J., 1997. Sedimentology and sequence stratigraphy of the Shanxi Formation (Lower Permian) in the northwestern Ordos Basin, China: an alternative sequence model for fluvial strata. *Sedimentary Geology*, 112: 123–136.

Zou Caineng, Dong Dazhong, Wang Shejiao, Li Jianzhong, Li Xinjing, Wang Yuman, Li Denghua and Cheng Keming, 2010. Geological characteristics and resource potential of shale gas in China. *Petroleum Exploration and Development*, 37: 641–653.

Zuo Zhaoxi, Zhang Xiaobo, Chen Shangbin, Si Qinghong, Zhang Chao and Liu Zheng, 2017. Heterogeneity of shale gas reservoirs in coal measures: a case study of the Taiyuan and shanxi Formations in the Ningwu Basin. *Acta Geologica Sinica,* 91:1130–1140 (in Chinese with English abstract).

About the first author

CHEN Qian, male; born in 1990; Ph.D., received a doctoral degree in China University of Geosciences (Beijing) in 2017 and is currently conducting post-doctoral research in the SINOPEC Petroleum Exploration and Production Institute. He majors at petroleum geology and his research interest focuses on oil and gas exploration especially unconventional natural gas resources. E-mail: chenqian.syky@.sinopec.com.